

Effects of charged Higgs bosons in the deep inelastic process $\nu_\tau \mathcal{N} \rightarrow \tau^- X$ and the possibility of detecting tau-neutrinos at cosmic neutrino detectors

M.I. Pedraza-Morales^(a), A. Rosado^(a) and H. Salazar^(b)

^(a) *Instituto de Física, BUAP. Apdo. Postal J-48, C.P. 72570 Puebla, Pue., México,*

^(b) *FCFM-BUAP. Apdo. Postal 1364, C.P. 72000 Puebla, Pue., México*

(Dated: December 14, 2018)

Abstract

We study the deep inelastic process $\nu_\tau + \mathcal{N} \rightarrow \tau^- + X$ (with $\mathcal{N} \equiv (n + p)/2$ an isoscalar nucleon), in the context of the two Higgs doublet model type II (2HDM(II)). We discuss the contribution to the total cross section of diagrams, in which a charged Higgs boson is exchanged. We present results which show the strong dependence of such contribution on $\tan \beta$ and M_{H^\pm} . We show that in the region $50 \leq \tan \beta \leq 200$ and $90 \text{ GeV} \leq M_{H^\pm} \leq 600 \text{ GeV}$ with the additional experimental constraint on the involved model parameters $M_{H^\pm} \geq 1.5 \times \tan \beta \text{ GeV}$, the contribution of the charged Higgs boson exchange diagrams to the cross section of the charged current inclusive $\nu_\tau \mathcal{N}$ collision can become important. We obtain that this contribution for an inclusive dispersion generated through the collision of an ultrahigh energy tau-neutrino with $E_\nu \approx 10^{20} \text{ eV}$ on a target nucleon can be larger than the value of the contribution of the W^\pm exchange diagrams, provided that $M_{H^\pm} \approx 300 \text{ GeV}$ and $\tan \beta \approx 200$. Such enhancement and the induced variation on the mean inelasticity $\langle y \rangle^{CC}$ could lead to sizeable effects in the acceptance of cosmic tau-neutrino detectors at experiments such as HiRes, PAO, and the CRTNT, which are anchored to the ground, and at experiments such as EUSO and OWL, which are proposed to orbit around the Earth. We also compare the contribution to $\sigma_{H^+}^{tot}$ from the different allowed initial quarks and we show that the contribution from the bottom quark dominates by far. This means that the H^\pm contribution practically always gives a top quark in the final state. Such a large component of the cross section having a top quark event in the final state could have recognizable features in the EAS experiments.

PACS numbers: 13.15.+g, 13.85.Tp, 14.60.Fg, 14.80.Cp, 95.55.Vj

I. INTRODUCTION.

Although the Standard Model (SM) [1], of the strong and electroweak interactions describes correctly Particle Physics at energy ranges currently attainable, one of its basic ingredients, the scalar Higgs sector, still remains untested. In the SM, the Higgs sector consists of a single $SU(2)$ doublet, and after spontaneous symmetry breaking (SSB) it remains a physical state, the Higgs boson (h_{sm}^0), whose mass is not predicted in the theory. On the other hand, the SM is not expected to be the ultimate theoretical structure responsible for electroweak symmetry breaking (EWSB) [2, 3]. One of the most simple extensions of the SM is the so called two Higgs doublet model (2HDM). There are four classes of 2HDM which naturally avoid tree-level flavor-changing neutral currents that can be induced by Higgs boson exchange [4]. These models include a Higgs sector with two scalar doublets, which give masses to the up and down-type fermions as well as the gauge bosons. Model II is particularly interesting, where one of the Higgs scalar doublet couples to the up-components of isodoublets while the other to the down-components. Model II is that utilized in SUSY theories. The 2HDM(II) has a rich structure and predicts interesting phenomenology [2]. The physical spectrum consists of two neutral CP-even states (h^0, H^0) and one CP-odd (A^0), as well as a pair of charged scalar particles (H^\pm). The advantage of such model is the fact that any Higgs sector built only upon doublets preserves naturally the lowest-order electroweak relation $\rho = 1$, with $\rho = M_{W^\pm}^2 / (M_Z^2 \cos^2 \theta)$, which has been tested with a good accuracy. On the phenomenological side, an important aspect of the 2HDM is that the Higgs sector may provide an additional source of CP violation [5].

Several experimental lower limits on the charged Higgs boson mass in this model have been reported in the literature:

$$M_{H^\pm} > 79.3 \text{ GeV} \quad (95\% \text{ C.L.}) [6], \quad (1)$$

$$M_{H^\pm} > (0.97, 1.28, 1.89) \times \tan \beta \text{ GeV} \quad (95\% \text{ C.L.}) [7], [8], [9], \quad (2)$$

$$M_{H^\pm} > (0.97, 1.5, 1.9, 2.5, 2.6) \times \tan \beta \text{ GeV} \quad (90\% \text{ C.L.}) [10], [11], [12], [13], [14]. \quad (3)$$

Further, based on the discussions on $\tan \beta$ given in Refs. [15] and [16], we restrict ourselves by taking the following upper limit on $\tan \beta$

$$\tan \beta \leq 200. \quad (4)$$

Large-scale neutrino telescopes [17] have as a main goal the detection of ultrahigh-energy (UHE) cosmic neutrinos ($E_\nu \geq 10^{12}$ eV) produced outside the atmosphere (neutrinos produced by galactic cosmic rays interacting with interstellar gas, and extragalactic neutrinos) [18, 19]. UHE neutrinos can be detected by observing long-range muons and tau-leptons decays produced in charged-current neutrino-nucleon interactions. UHE tau-neutrinos are generated through neutrino oscillations [20, 21]. The detection of UHE neutrinos will provide us with the possibility to observe $\nu\mathcal{N}$ -collisions with a neutrino energy in the range $10^{12} \text{ eV} \leq E_\nu \leq 10^{21} \text{ eV}$ and a target nucleon at rest. An enlightening discussion on UHE neutrino interactions is given by R. Gandhi *et al.* [19].

We discuss in this paper the cross section of the deep inelastic process $\nu_\tau + \mathcal{N} \rightarrow \tau^- + X$ ($\mathcal{N} \equiv (n + p)/2$ an isoscalar nucleon), in the context of the SM and of the 2HDM(II). We perform our numerical calculations using the parton model [22, 23] with the parton distribution functions reported by J. Pumplin *et al.* [24]. We use the CTEQ PDFs provided in an $n_f = 5$ active flavors scheme. Our aim is to calculate how large can be the contribution of diagrams, in which a charged Higgs boson is exchanged, to the total cross section of the mentioned inclusive process in the frame of the 2HDM(II). In the 2HDM(II) the couplings of the down-type quarks and charged leptons are proportional to $m_f \times \tan\beta$. Hence, for large $\tan\beta$ the contribution of H^\pm -exchange diagrams will be maximal in this model.

This paper is organized as follows. In section II, we review the notation and physical region of the inclusive $\nu_t\mathcal{N}$ -dispersion. In section III, we present the formulae for the differential cross section of the deep inelastic process $\nu_\tau\mathcal{N} \rightarrow \tau^- + X$, in the context of the SM and the 2HDM(II). In section IV, we give and discuss our results for the total cross section rates of the charged current deep inelastic process $\nu_\tau\mathcal{N}$ in the frame of the SM and 2HDM(II). In section V, we discuss the contribution of charged Higgs boson to the charged current cross section of the $\nu_\tau\mathcal{N}$ collision, the induced variation on the mean inelasticity $\langle y \rangle^{CC}$ and hence the effects on the possibility of detecting cosmic tau-neutrinos. Finally, in section VI, we summarize our conclusions.

II. NOTATION, PHYSICAL REGION

In this section we review the notation and the physical region for the parameters of the inclusive process

$$\nu_l + \mathcal{N} \rightarrow l^- + X, \quad (5)$$

where ν_l , \mathcal{N} , and l^- stand for the incoming neutrino, the target nucleon and the outgoing lepton l^- , respectively. We will denote the four-momenta of these particles by p , $P_{\mathcal{N}}$ and p' , respectively. In accordance with the kinematics for the collision of a neutrino on a target nucleon, the following construction is chosen:

$$p^\mu = E_\nu(1, 0, 0, 1), \quad P_{\mathcal{N}}^\mu = M_{\mathcal{N}}(1, 0, 0, 0). \quad (6)$$

As usual, we define the invariants [23]:

$$\begin{aligned} s &= (p + P_{\mathcal{N}})^2, \\ Q^2 &= -(p - p')^2, \\ \nu &= P_{\mathcal{N}}(p - p')/M_{\mathcal{N}}, \end{aligned} \quad (7)$$

and the dimensionless variables:

$$x = \frac{Q^2}{2\nu M_{\mathcal{N}}}, \quad y = \frac{\nu}{E_\nu}. \quad (8)$$

The physical region of these kinematical variables is obtained by requiring that the scalar products of any two particle four-momenta be positive and the determinant Δ_3 of the three independent four-momenta (whenever possible we will neglect the fermion masses):

$$\Delta_3(p, p', P_{\mathcal{N}}) = \begin{vmatrix} 0 & pp' & pP_{\mathcal{N}} \\ p'p & 0 & p'P_{\mathcal{N}} \\ P_{\mathcal{N}}p & P_{\mathcal{N}}p' & 0 \end{vmatrix} \quad (9)$$

be positive [25].

From the non-negative character of the scalar products we find:

$$0 \leq x \leq 1, \quad 0 \leq y \leq 1. \quad (10)$$

Explicit evaluation of Δ_3 using (7), (8) and (9) gives:

$$\Delta_3 = (s/2)^3 2xy(1 - y). \quad (11)$$

with $s = 2M_{\mathcal{N}}E_{\nu}$. The condition $\Delta_3 \geq 0$ does not lead to additional restrictions on the physical region.

The expressions given in (10), define the physical region for the dimensionless variables x , and y . We have taken all fermion masses to be zero, which implies that in the calculation of the total cross section the integration over the momentum transfer square extends up to zero. However, the parton distributions can be used only when Q^2 is not too small. Furthermore, in order to separate deep inelastic from elastic scattering, a cut on the invariant mass W of the unobserved particles in the final state is required. Therefore, besides the kinematical conditions (10), we also have in general the following constraints:

$$\begin{aligned} Q^2 &= sxy \geq Q_c^2, \\ W &= sy(1-x) \geq W_c. \end{aligned} \quad (12)$$

The cuts for Q^2 and W constrain further the physically allowed region for the process (5). The physical region can now be written in terms of the dimensionless variables as follows:

$$\frac{Q_c^2}{s} \leq x \leq 1 - \frac{W_c}{s}, \quad \max \left\{ \frac{Q_c^2}{sx}, \frac{W_c}{s(1-x)} \right\} \leq y \leq 1. \quad (13)$$

The physically allowed region can also be expressed as

$$\frac{Q_c^2 + W_c}{s} \leq y \leq 1, \quad \frac{Q_c^2}{sy} \leq x \leq 1 - \frac{W_c}{sy}. \quad (14)$$

III. THE CROSS SECTION FOR THE INCLUSIVE PROCESS $\nu_{\tau} + \mathcal{N} \rightarrow \tau^{-} + X$

A. The differential cross section for the process $\nu_{\tau} + \mathcal{N} \rightarrow \tau^{-} + X$ in the SM

The differential cross section for the inclusive reaction

$$\nu_{\tau}(p) + \mathcal{N}(P_{\mathcal{N}}) \rightarrow \tau^{-}(p') + X, \quad (15)$$

where $\mathcal{N} \equiv (n + p)/2$ is an isoscalar nucleon, at the lowest order in α in the frame of the SM (see Fig. 1) is given as follows [26]:

$$\frac{d^2\sigma_{sm}}{dxdy} = \frac{2G_F^2 M_{\mathcal{N}} E_{\nu}}{\pi} \left(\frac{M_{W^{\pm}}^2}{Q^2 + M_{W^{\pm}}^2} \right)^2 [xq_W(x, Q^2) + x\bar{q}_W(x, Q^2)(1-y)^2], \quad (16)$$

where Q^2 , x and y are defined in (7) and (8) and M_N stands for the nucleon mass. The quantities $q_W(x, Q^2)$ and $\bar{q}_W(x, Q^2)$ are given as

$$\begin{aligned} q_W(x, Q^2) &= \frac{u_v(x, Q^2) + d_v(x, Q^2)}{2} \\ &\quad + \frac{u_s(x, Q^2) + d_s(x, Q^2)}{2} + s_s(x, Q^2) + b_s(x, Q^2), \\ \bar{q}_W(x, Q^2) &= \frac{u_s(x, Q^2) + d_s(x, Q^2)}{2} + c_s(x, Q^2), \end{aligned} \quad (17)$$

where the valence and sea parton distribution functions (PDFs), $q_v(x, Q^2)$ and $q_s(x, Q^2)$, can be expressed as

$$\begin{aligned} u_v(x, Q^2) &= u(x, Q^2) - \bar{u}(x, Q^2), \\ d_v(x, Q^2) &= d(x, Q^2) - \bar{d}(x, Q^2), \\ u_s(x, Q^2) &= \bar{u}(x, Q^2), \\ d_s(x, Q^2) &= \bar{d}(x, Q^2), \\ c_s(x, Q^2) &= c(x, Q^2) = \bar{c}(x, Q^2), \\ s_s(x, Q^2) &= s(x, Q^2) = \bar{s}(x, Q^2), \\ b_s(x, Q^2) &= b(x, Q^2) = \bar{b}(x, Q^2), \end{aligned} \quad (18)$$

where the PDFs $q(x, Q^2)$ describe the quark q content of the proton. In other words, the parton distribution functions $q(x, Q^2)$ give the probabilities to find a quark q inside a proton with the fraction x of the proton momentum: $q^\mu = xP^\mu$, in a scattering process with momentum transfer square Q^2 .

In the case of the standard model the couplings of the fermions to the W^\pm boson are given by the lagrangian

$$\mathcal{L} = -\frac{g}{\sqrt{2}} \sum_{(f_u, f_d)} \left\{ \left(\bar{f}_u \gamma^\mu \frac{1 - \gamma_5}{2} f_d \right) W_\mu^+ + \left(\bar{f}_d \gamma^\mu \frac{1 - \gamma_5}{2} f_u \right) W_\mu^- \right\}, \quad (19)$$

where f_u and f_d stand for the up- and down-components of the fermion doublet.

B. The differential cross section for the process $\nu_\tau + N \rightarrow \tau^- + X$ in the 2HDM(II)

The differential cross section for the inclusive reaction (15), at the lowest order in α in the frame of the 2HDM(II) (see Fig. 2), can be written as follows [27]:

$$\frac{d^2 \sigma_{2hdm}}{dx dy} = \frac{d^2 \sigma_{sm}}{dx dy} + \frac{d^2 \sigma_{H^+}}{dx dy}, \quad (20)$$

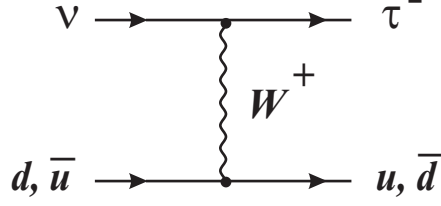


FIG. 1: Diagrams which at the quark level contribute to the process $\nu_\tau + \mathcal{N} \rightarrow \tau^- + X$ at the lowest order in α in the SM (d stands for d -, s - and b -quark; and u stands for u - and c -quark).

where for large $\tan \beta$

$$\frac{d^2 \sigma_{H^+}}{dx dy} = \frac{G_F^2 M_{\mathcal{N}} E_\nu}{2\pi} \frac{m_\tau^2 M_{W^\pm}^2 \tan^4 \beta}{(Q^2 + M_{H^\pm}^2)^2} y^2 [x q_H(x, Q^2) + x \bar{q}_H(x, Q^2)], \quad (21)$$

where Q^2 , x and y are defined in (7) and (8) and $M_{\mathcal{N}}$ stands for the nucleon mass. The quantities $q_W(x, Q^2)$ and $\bar{q}_W(x, Q^2)$ are given in (17), whereas $q_H(x, Q^2)$ and $\bar{q}_H(x, Q^2)$ are given as

$$\begin{aligned} q_H(x, Q^2) &= \frac{m_d^2}{M_{W^\pm}^2} \left(\frac{u_v(x, Q^2) + d_v(x, Q^2)}{2} + \frac{u_s(x, Q^2) + d_s(x, Q^2)}{2} \right) \\ &\quad + \frac{m_s^2}{M_{W^\pm}^2} s_s(x, Q^2) + \frac{m_b^2}{M_{W^\pm}^2} b_s(x, Q^2) \\ \bar{q}_H(x, Q^2) &= \frac{m_d^2}{M_{W^\pm}^2} \left(\frac{u_s(x, Q^2) + d_s(x, Q^2)}{2} \right) + \frac{m_s^2}{M_{W^\pm}^2} c_s(x, Q^2). \end{aligned} \quad (22)$$

In the case of the 2HDM(II) the couplings of the fermions to the W^\pm boson are given by the lagrangian in Eq.(19), in a way similar to the SM [2]. On the other side, taking the elements of the CKM-matrix $V_{ij} = \delta_{ij}$, the couplings of the fermions to the H^\pm boson are given by the lagrangian [2]

$$\mathcal{L} = \frac{g}{M_{W^\pm}} \left\{ m_\tau \tan \beta \left(\bar{\nu} \frac{1 + \gamma_5}{2} \tau \right) + m_u \cot \beta \left(\bar{u} \frac{1 - \gamma_5}{2} d \right) + m_d \tan \beta \left(\bar{u} \frac{1 + \gamma_5}{2} d \right) \right\} H^+ + h.c. \quad (23)$$

IV. RESULTS FOR DEEP INELASTIC $\nu_\tau \mathcal{N}$ IN THE SM AND THE 2HDM(II)

We present results for the case of unpolarized deep inelastic process $\nu_\tau + \mathcal{N} \rightarrow \tau^- + X$ with a neutrino energy in the range $10^{14} \text{ eV} \leq E_\nu \leq 10^{20} \text{ eV}$ and the nucleon at rest, *i.e.* a target nucleon. We take $10^{14} \text{ eV} \leq E_\nu$ which leads to a condition where all fermion masses

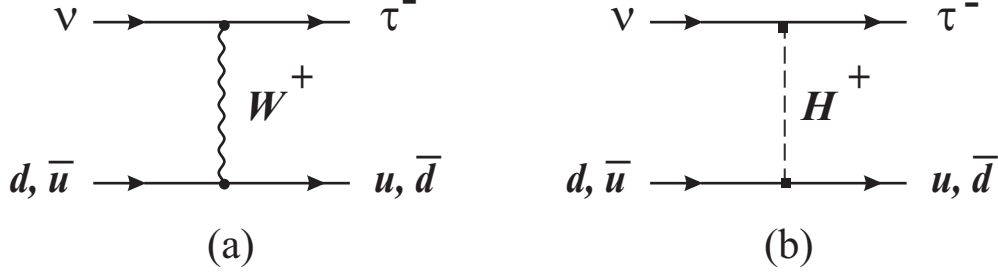


FIG. 2: Diagrams which at the quark level contribute to the process $\nu_\tau + \mathcal{N} \rightarrow \tau^- + X$ at the lowest order in α in the 2HDM(II) (d stands for d -, s - and b -quark; and u stands for u - and c -quark).

become negligible with respect to the total energy $s = 2M_{\mathcal{N}}E_\nu$, even the top quark mass. We take cuts of $\sim 2 \text{ GeV}^2$ and 10 GeV^2 for Q^2 and the invariant mass W , respectively. These values for the cuts are suited for the parton distribution functions of J. Pumplin *et al.* [24] which we will use in our calculations. We have checked numerically that the total cross section rates do not depend on the choice of the cuts on the momentum transfer square Q^2 , when they take on values of a few GeV^2 . This is due to the fact that the propagators involved in the calculation of the cross section are $1/(M_{W^\pm}^2 + Q^2)$ and $1/(M_{H^\pm}^2 + Q^2)$.

We perform our numerical calculations taking for the quark masses: $m_u = 4 \text{ MeV}$, $m_d = 8 \text{ MeV}$, $m_c = 1.5 \text{ GeV}$, $m_s = 150 \text{ MeV}$, $m_b = 4.9 \text{ GeV}$ and $m_t = 174 \text{ GeV}$. For the evaluation of the $H^\pm \tau^- \nu_\tau$ coupling we take $m_{\nu_\tau} = 0$ and $m_\tau = 1,777 \text{ MeV}$. Also, we take $M_{W^\pm} = 80.4 \text{ GeV}$ for the mass of the charged boson W^\pm [28]

Taking into account the constraints on $M_{H^\pm}/\tan\beta$ given by (2) and (3), we will present results for three different cases: (I) $M_{H^\pm} = 1.5 \tan\beta \text{ GeV}$; (II) $M_{H^\pm} = 2.0 \tan\beta \text{ GeV}$; (III) $M_{H^\pm} = 3.0 \tan\beta \text{ GeV}$. In all these cases, the conditions (1) and (4) will be fulfilled. Hence, we restrict our numerical analysis to the region $50 \leq \tan\beta \leq 200$ and $90 \text{ GeV} \leq M_{H^\pm} \leq 600 \text{ GeV}$.

A. Total cross section σ_{sm}^{tot} and σ_{2hdm}^{tot}

We display in our numerical results for the total cross section as a function of E_ν in the range $10^{14} \text{ eV} \leq E_\nu \leq 10^{20} \text{ eV}$, with $E_{\mathcal{N}} = M_{\mathcal{N}}$ in Tables I-III. In the second column of these Tables we give results for the SM. The numerical results for the 2HDM(II) are given in the third-sixth columns of Table I (Case I), Table II (Case II), and Table III (Case III).

Tables I, II and III show that the total cross section σ_{2hdm}^{tot} becomes larger as $\tan\beta$ increases and/or as M_{H^\pm} decreases.

B. The ratio $\sigma_{H^+}^{tot}(\nu_\tau + \mathcal{N} \rightarrow \tau^- + X)/\sigma_{sm}^{tot}(\nu_\tau + \mathcal{N} \rightarrow \tau^- + X)$

We present in our results for the ratio $\sigma_{H^+}^{tot}(\nu_\tau + \mathcal{N} \rightarrow \tau^- + X)/\sigma_{sm}^{tot}(\nu_\tau + \mathcal{N} \rightarrow \tau^- + X)$ as a function of E_ν in the range $10^{14} \text{ eV} \leq E_\nu \leq 10^{20} \text{ eV}$, with $E_{\mathcal{N}} = M_{\mathcal{N}}$, in Table IV (Case I), Table V (Case II), and Table VI (Case III).

We observe in Tables IV, V and VI that the ratio $\sigma_{H^+}^{tot}/\sigma_{sm}^{tot}$ becomes larger as $\tan\beta$ increases and/or as M_{H^\pm} decreases. Furthermore, we notice that $\sigma_{H^+}^{tot}/\sigma_{sm}^{tot}$ depends on E_ν . We see that for $\tan\beta = 150$ and $\tan\beta = 200$, the greater E_ν , the larger ratio $\sigma_{H^+}^{tot}/\sigma_{sm}^{tot}$ becomes.

C. Comparison of the contribution to $\sigma_{H^+}^{tot}$ from the different quarks

Finally, in Table VII we compare the contribution to $\sigma_{H^+}^{tot}$ from the different allowed initial quarks (see Fig. 2(b)), taking $M_{H^\pm} = 400 \text{ GeV}$ and $\tan\beta = 200$. We observe in this table that the contribution from the bottom quark dominates by far (a similar behavior is obtained in the other cases). This fact implies that the contribution of the H^\pm exchange diagrams to the total cross section of the $\nu_\tau \mathcal{N}$ scattering in the frame of the 2HDM(II) is the same regardless of whether the nucleon is a proton, a neutron or an isoscalar nucleon, because these particles have the same content of b-quark. We would like to emphasize that the H^\pm contribution practically always gives a top quark in the final state, resulting in a much larger values of the mass invariant W and dimensionless parameter y in the 2HDM with respect to the corresponding values in the case of the SM. Such a large component of the cross section having a top quark event in the final state could have other recognizable features in the EAS experiments, which may be worth looking into.

V. CHARGED HIGGS BOSON EFFECTS IN THE POSSIBILITY OF DETECTING ULTRA-HIGH ENERGY TAU-NEUTRINOS

Cosmic neutrino fluxes can initiate air-showers through interaction in the atmosphere, or in the Earth. Neutrino trajectories will be going down in a nearly horizontal way in the former case, whereas in a Earth-skimming manner in the latter case. Thus, it is important to know the acceptance (event rate/flux) of proposed air shower experiments for detecting both types of neutrino -initiated events [Horizontal air-showers (HAS) and Up-going (Earth-skimming) air-showers (UAS)]. These acceptances for fluorescence detectors have been calculated in [29] for experiments as High Resolution Fly's Eye Detector (HiRes) [30], Pierre Auger Observatory (PAO) [31], and the Cosmic Ray Tau Neutrino Telescopes (CRTNT) [32], which are anchored to the ground, and at experiments as Extreme Universe Space Observatory (EUSO) [33] and Orbiting wide angle light-collectors (OWL) [34], which are proposed to orbit around the Earth. In Ref.[29], it is stated that the very different dependence on the cross section of the HAS (linear) and UAS (non linear) acceptances will provide a practical method to measure the charged current cross section of the neutrino nucleon scattering $\sigma_{\nu\mathcal{N}}^{CC}$. One simply has to exploit the ratio of UAS to HAS event rates. However, one assumption made in Ref.[29] was taking that $\sigma_{\nu_e\mathcal{N}}^{CC} = \sigma_{\nu_\mu\mathcal{N}}^{CC} = \sigma_{\nu_\tau\mathcal{N}}^{CC}$. This is valid in the SM, but it is no longer valid in the 2HDM(II), because the $\sigma_{\nu_\tau\mathcal{N}}^{CC}$ could be twice larger than $\sigma_{\nu_e\mathcal{N}}^{CC} = \sigma_{\nu_\mu\mathcal{N}}^{CC}$ in this model. Hence, the neutrino charged current interaction mean-free path (introduced in Ref.[29]) could be for ν_τ one half of that for ν_e and ν_μ , in the mentioned model. Therefore, the existence of charged Higgs bosons could imply a large deviation from the results for the acceptances for space based (or ground based) tau-neutrino detectors presented in Fig. 7 of Ref.[29].

Further, it was already pointed out in Ref.[35], that besides the obvious role of the neutrino cross section in the actual interaction that leads to the possible neutrino detection there are other more subtle effects. The y distribution of the cross section also has an impact on the detection rate [35, 36, 37]. It is clear from Eq.(16) and Eq.(21) that the y distribution of the charged current interaction could change due to the effects of charged Higgs bosons. In fact, in Table VIII we show how the mean inelasticity $\langle y \rangle^{CC}$ would change in the THDM(II) (We present only numerical results for the Case I, in which the effects are maximal). Our results obtained for $\langle y \rangle^{CC}$ in the frame of the SM are in good agreement

with those reported in Ref.[38]. We observe in Table VIII that $\langle y \rangle_{2hdm}^{CC} \cong 2.5 \times \langle y \rangle_{sm}^{CC}$ for $M_{H^\pm} = 300$ GeV, $\tan \beta = 200$ and $E_\nu = 10^{20}$ eV. Such a drastic variation in $\langle y \rangle^{CC}$ could induce a large variation in the possibility of detecting ultra-high energy tau-neutrinos through inclined showers [35]. We end this section saying that the possible effects of charged Higgs bosons on the detection of cosmic tau-neutrinos deserve future detailed investigations.

VI. CONCLUSIONS

We have calculated the total cross section rates for the deep inelastic process $\nu_\tau + \mathcal{N} \rightarrow \tau^- + X$, where $\mathcal{N} \equiv (n + p)/2$ is an isoscalar nucleon, in the frame of the SM and the 2HDM(II). In the case of the 2HDM(II) we have taken into account the contribution of the diagrams in which a charged Higgs boson is exchanged $\sigma_{H^\pm}^{tot}$.

We obtained our numerical results considering the nucleon at rest and according to the following conditions: taking $M_{W^\pm} = 80.4$ GeV, $\sin^2 \theta_W = 0.223$, a neutrino energy in the range $10^{14} \text{ eV} \leq E_\nu \leq 10^{20} \text{ eV}$ and setting cuts of $\sim 2 \text{ GeV}^2$ and 10 GeV^2 for the momentum transfer square Q^2 and the invariant mass (W), respectively. We made use of the parton distribution functions of J. Pumplin *et al.*, those provided in an $n_f = 5$ active flavors scheme. In order to take into account the experimental data, we restricted our numerical analysis to the region $50 \leq \tan \beta \leq 200$ and $90 \text{ GeV} \leq M_{H^\pm} \leq 600 \text{ GeV}$, with the additional constraint $M_{H^\pm} \geq 1.5 \times \tan \beta \text{ GeV}$.

We have shown that the most important contribution to $\sigma_{H^\pm}^{tot}$ comes from the H^\pm -exchange diagram with an initial b-quark (and hence an outgoing t-quark). This fact implies that the contribution of the H^\pm exchange diagrams to the total cross section of the $\nu_\tau \mathcal{N}$ scattering in the frame of the 2HDM(II) is the same regardless of whether the nucleon is a proton, a neutron or an isoscalar nucleon, because these particles have the same content of b-quark. On the other hand, we would like to stress that the H^\pm contribution leads to a top quark in the final state and that such a large component of the cross section having a top quark event in the final state could have characteristic aspects in the EAS experiments.

We found that the ratio $\sigma_{H^\pm}^{tot}/\sigma_{sm}^{tot}$ becomes larger as $\tan \beta$ increases and/or as M_{H^\pm} decreases. We also found that the ratio $\sigma_{H^\pm}^{tot}/\sigma_{sm}^{tot}$ depends on E_ν . In particular, we obtain that for $\tan \beta = 150$ and $\tan \beta = 200$: the greater E_ν , the larger ratio $\sigma_{H^\pm}^{tot}/\sigma_{sm}^{tot}$ becomes.

We showed that the contribution of the charged Higgs boson exchange diagrams can

lead to a sizeable enhancement with respect to the SM cross section rates for the charged current $\nu_\tau \mathcal{N}$ deep inelastic scattering. For the case of an ultrahigh energy tau-neutrino with $E_\nu = 10^{20}$ eV colliding on a target nucleon such enhancement reached 110% provided that $\tan \beta = 200$ and $M_{H^\pm} = 300$ GeV. Besides, we obtain $\langle y \rangle_{2hdm}^{CC} \approx 2.5 \times \langle y \rangle_{sm}^{CC}$ for the same values of E_ν , $\tan \beta$ and M_{H^\pm} . This enhancement and the induced variation in the mean inelasticity $\langle y \rangle^{CC}$ could lead to sizeable effects in the acceptance of the cosmic tau-neutrino detectors at space based experiments such as the EUSO and OWL proposals and at ground-based experiments such as PAO, HiRes and the CRTNT.

ACKNOWLEDGMENTS

The authors are grateful to *Sistema Nacional de Investigadores* and *CONACyT* (México) for financial support and also to Dr. Antonio Flores-Riveros for a careful and critical reading of the manuscript. A.R. would like to thank Prof. D.P. Roy for valuable comments.

-
- [1] S. L. Glashow, Nucl. Phys. **22**, 579 (1961); S. Weinberg, Phys. Rev. Lett. **19**, 1264 (1967); A. Salam, Proc. 8th NOBEL Symposium, ed. N. Svartholm (Almqvist and Wiksell, Stockholm, 1968), p. 367.
 - [2] J. Gunion, H. Haber, G. Kane and S. Dawson, *The Higgs Hunter's Guide*, Addison-Wesley Publishing Company, Reading, MA, 1990.
 - [3] H. E. Haber, in *Testing the Standard Model*, Proceedings of the 1990 Theoretical Advanced Study Institute in Elementary Particle Physics, edited by M. Cvetič and P. Langacker (World Scientific, Singapore, 1991) p. 340-475.
 - [4] V. D. Barger, J. L. Hewett and R. J. N. Phillips, Phys. Rev. D **41**, 3421 (1990).
 - [5] T. D. Lee, Phys. Rev. D **8**, 1226 (1973); T. D. Lee, Phys. Rept. **9**, 143 (1974); S. Weinberg, Phys. Rev. Lett. **37**, 657 (1976); Y. L. Wu and L. Wolfenstein, Phys. Rev. Lett. **73**, 1762 (1994) [arXiv:hep-ph/9409421]; J. Liu and L. Wolfenstein, Nucl. Phys. B **289**, 1 (1987).
 - [6] A. Heister *et al.* [ALEPH Collaboration], Phys. Lett. B **543**, 1 (2002) [arXiv:hep-ex/0207054].
 - [7] K. Ackerstaff *et al.* [OPAL Collaboration], Eur. Phys. J. C **8**, 3 (1999) [arXiv:hep-ex/9808016].
 - [8] G. Abbiendi *et al.* [OPAL Collaboration], Phys. Lett. B **551**, 35 (2003) [arXiv:hep-ex/0211066].

- [9] G. Abbiendi *et al.* [OPAL Collaboration], Phys. Lett. B **520**, 1 (2001) [arXiv:hep-ex/0108031].
- [10] R. Ammar *et al.* [CLEO Collaboration], Phys. Rev. Lett. **78**, 4686 (1997).
- [11] A. Stahl and H. Voss, Z. Phys. C **74**, 73 (1997).
- [12] D. Buskulic *et al.* [ALEPH Collaboration], Phys. Lett. B **343**, 444 (1995).
- [13] R. Barate *et al.* [ALEPH Collaboration], Eur. Phys. J. C **19**, 213 (2001) [arXiv:hep-ex/0010022].
- [14] M. Acciarri *et al.* [L3 Collaboration], Phys. Lett. B **396**, 327 (1997).
- [15] D. P. Roy, AIP Conf. Proc. **805**, 110 (2006) [arXiv:hep-ph/0510070].
- [16] H. Baer, J. Ferrandis and X. Tata, Phys. Lett. B **561**, 145 (2003) [arXiv:hep-ph/0211418].
- [17] *AMANDA Collaboration*, E. Andres *et al.*, Nature **410**, 441 (2001); *ANTARES Collaboration*, Y. Becherini *et al.*, e-Print Archive: hep-ph/0211173; *AUGER Collaboration*, D. Zavrtanik *et al.*, Nucl. Phys. Proc. Suppl. **85**, 324 (2002); *NESTOR Collaboration*, P. K. F. Grieder *et al.*, Nuovo Cim. **24C**, 771 (2001); *RICE Collaboration*, I. Kravchenko *et al.*, Astropart. Phys. **19**, 15 (2003).
- [18] V. S. Beresinsky and G. T. Zatsepin, Phys. Lett. B **28**, 423 (1969); V. S. Berezinsky and V. I. Dokuchaev, Nucl. Phys. Proc. Suppl. **110**, 522 (2002); V. S. Berezinsky, Nucl. Phys. Proc. Suppl. **38**, 363 (1995); and Nucl. Phys. Proc. Suppl. **31**, 413 (1993); T. Stanev, Nucl. Phys. Proc. Suppl. **14A**, 17 (1990); K. Greisen, Phys. Rev. Lett. **16**, 748 (1966); C. T. Hill and D. N. Schramm, Phys. Lett. B **131**, 247 (1983); and Phys. Rev. D **31**, 564 (1985).
- [19] R. Gandhi, C. Quigg, M. H. Reno and I. Sarcevic, Phys. Rev. D **58**, 093009 (1998) [arXiv:hep-ph/9807264].
- [20] O. Blanch and P. Billoir, "Acceptance and Flux Limit for ν_τ with the Pierre Auger Observatory Surface Detector", Preprint LPNHE, Paris (France), September 26, 2005.
- [21] X. Bertou, P. Billoir, O. Deligny, C. Lachaud and A. Letessier-Selvon, Astropart. Phys. **17**, 183 (2002) [arXiv:astro-ph/0104452].
- [22] R. P. Feynman: Photon-hadron interactions. Reading: Benjamin 1972.
- [23] V.D. Barger and R.J.N. Phillips, Collider Physics (Updated Edition), Addison-Wesley Publishing Company, Inc., Reading, Massachusetts, 1997.
- [24] J. Pumplin *et al.*, JHEP **207**, 12 (2002); D. Stump *et al.*, e-Print Archive: hep-ph/0303013.
- [25] E. Byckling and Kajantie: Particle kinematics. New York: Willey 1972.
- [26] M. H. Reno and C. Quigg, Phys. Rev. D **37**, 657 (1988); C. Quigg, M. H. Reno and

- T. P. Walker, Phys. Rev. Lett. **57**, 774 (1986).
- [27] A. Rosado, Phys. Rev. D **74**, 057301 (2006).
- [28] S. Eidelman *et al.* [Particle Data Group], Phys. Lett. B **592**, 1 (2004).
- [29] S. Palomares-Ruiz, A. Irimia and T. J. Weiler, Phys. Rev. D **73**, 083003 (2006) [arXiv:astro-ph/0512231].
- [30] P. Sokolsky and J. Belz [the HiRes Collaboration], “Comparison of UHE composition measurements by Fly’s Eye, HiRes-prototype / MIA and stereo HiRes experiments,” arXiv:astro-ph/0507485.
- [31] H. Blumer *et al.* [Auger Collaboration], “The Auger fluorescence detector prototype telescope,” FZKA-6345P *Prepared for 26th International Cosmic Ray Conference (ICRC 99), Salt Lake City, UT, 17-25 Aug 1999*; J. Abraham *et al.* [Pierre Auger Collaboration], Nucl. Instrum. Meth. A **523**, 50 (2004).
- [32] Z. Cao, Nucl. Phys. Proc. Suppl. **151**, 287 (2006).
- [33] Ph. Gorodetzky [The EUSO Collaboration], Nucl. Phys. Proc. Suppl. **151**, 401 (2006) [arXiv:astro-ph/0502187]; G. D’Ali Staiti [EUSO Collaboration], Nucl. Phys. Proc. Suppl. **136**, 415 (2004).
- [34] F. W. Stecker, J. F. Krizmanic, L. M. Barbier, E. Loh, J. W. Mitchell, P. Sokolsky and R. E. Streitmatter, Nucl. Phys. Proc. Suppl. **136C**, 433 (2004) [arXiv:astro-ph/0408162].
- [35] E. Zas, New J. Phys. **7**, 130 (2005) [arXiv:astro-ph/0504610].
- [36] R. Gandhi, C. Quigg, M. H. Reno and I. Sarcevic, Astropart. Phys. **5**, 81 (1996) [arXiv:hep-ph/9512364].
- [37] J. C. Arteaga-Velazquez and A. Zepeda, “Estimation of the detectable flux of astrophysical neutrinos at the Pierre Auger observatory by means of horizontal air showers,” *Proceedings of 29th International Cosmic Ray Conference Pune Vol. 9, 151-154 (2005)*.
- [38] C. Aramo, A. Insolia, A. Leonardi, G. Miele, L. Perrone, O. Pisanti and D. V. Semikoz, Astropart. Phys. **23**, 65 (2005) [arXiv:astro-ph/0407638].

$E_\nu(\text{eV})$	$\sigma_{sm}^{tot}(\text{cm}^2)$	$\sigma_{2hdm}^{tot}(\text{cm}^2)$			
		I(a)	I(b)	I(c)	I(d)
10^{14}	2.01×10^{-34}	2.17×10^{-34}	2.23×10^{-34}	2.27×10^{-34}	2.29×10^{-34}
10^{15}	6.86×10^{-34}	7.62×10^{-34}	8.22×10^{-34}	8.82×10^{-34}	9.28×10^{-34}
10^{16}	1.95×10^{-33}	2.19×10^{-33}	2.45×10^{-33}	2.79×10^{-33}	3.12×10^{-33}
10^{17}	4.93×10^{-33}	5.54×10^{-33}	6.33×10^{-33}	7.49×10^{-33}	8.75×10^{-33}
10^{18}	1.14×10^{-32}	1.28×10^{-32}	1.48×10^{-32}	1.79×10^{-32}	2.16×10^{-32}
10^{19}	2.44×10^{-32}	2.73×10^{-32}	3.19×10^{-32}	3.95×10^{-32}	4.87×10^{-32}
10^{20}	4.76×10^{-32}	5.27×10^{-32}	6.22×10^{-32}	7.89×10^{-32}	9.99×10^{-32}

TABLE I: Total cross section as a function of E_ν , with $E_N = M_N$. We compare σ_{sm}^{tot} with σ_{2hdm}^{tot} by taking: I(a) $M_{H^\pm} = 90$ GeV and $\tan \beta = 60$; I(b) $M_{H^\pm} = 150$ GeV and $\tan \beta = 100$; I(c) $M_{H^\pm} = 225$ GeV and $\tan \beta = 150$; I(d) $M_{H^\pm} = 300$ GeV and $\tan \beta = 200$.

$E_\nu(\text{eV})$	$\sigma_{sm}^{tot}(\text{cm}^2)$	$\sigma_{2hdm}^{tot}(\text{cm}^2)$			
		II(a)	II(b)	II(c)	II(d)
10^{14}	2.01×10^{-34}	2.06×10^{-34}	2.09×10^{-34}	2.10×10^{-34}	2.10×10^{-34}
10^{15}	6.86×10^{-34}	7.14×10^{-34}	7.43×10^{-34}	7.63×10^{-34}	7.77×10^{-34}
10^{16}	1.95×10^{-33}	2.04×10^{-33}	2.18×10^{-33}	2.32×10^{-33}	2.45×10^{-33}
10^{17}	4.93×10^{-33}	5.16×10^{-33}	5.61×10^{-33}	6.14×10^{-33}	6.69×10^{-33}
10^{18}	1.14×10^{-32}	1.19×10^{-32}	1.31×10^{-32}	1.46×10^{-32}	1.63×10^{-32}
10^{19}	2.44×10^{-32}	2.55×10^{-32}	2.83×10^{-32}	3.21×10^{-32}	3.66×10^{-32}
10^{20}	4.76×10^{-32}	4.96×10^{-32}	5.55×10^{-32}	6.41×10^{-32}	7.47×10^{-32}

TABLE II: Total cross section as a function of E_ν , with $E_N = M_N$. We compare σ_{sm}^{tot} with σ_{2hdm}^{tot} by taking: II(a) $M_{H^\pm} = 100$ GeV and $\tan \beta = 50$; II(b) $M_{H^\pm} = 200$ GeV and $\tan \beta = 100$; II(c) $M_{H^\pm} = 300$ GeV and $\tan \beta = 150$; II(d) $M_{H^\pm} = 400$ GeV and $\tan \beta = 200$.

$E_\nu(\text{eV})$	$\sigma_{sm}^{tot}(\text{cm}^2)$	$\sigma_{2hdm}^{tot}(\text{cm}^2)$			
		III(a)	III(b)	III(c)	III(d)
10^{14}	2.01×10^{-34}	2.02×10^{-34}	2.03×10^{-34}	2.03×10^{-34}	2.03×10^{-34}
10^{15}	6.86×10^{-34}	6.95×10^{-34}	7.01×10^{-34}	7.05×10^{-34}	7.07×10^{-34}
10^{16}	1.95×10^{-33}	1.98×10^{-33}	2.03×10^{-33}	2.06×10^{-33}	2.09×10^{-33}
10^{17}	4.93×10^{-33}	5.02×10^{-33}	5.17×10^{-33}	5.33×10^{-33}	5.50×10^{-33}
10^{18}	1.14×10^{-32}	1.16×10^{-32}	1.20×10^{-32}	1.25×10^{-32}	1.31×10^{-32}
10^{19}	2.44×10^{-32}	2.49×10^{-32}	2.59×10^{-32}	2.73×10^{-32}	2.89×10^{-32}
10^{20}	4.76×10^{-32}	4.85×10^{-32}	5.08×10^{-32}	5.41×10^{-32}	5.80×10^{-32}

TABLE III: Total cross section as a function of E_ν , with $E_{\mathcal{N}} = M_{\mathcal{N}}$. We compare σ_{sm}^{tot} with σ_{2hdm}^{tot} by taking: III(a) $M_{H^\pm} = 150$ GeV and $\tan \beta = 50$; III(b) $M_{H^\pm} = 300$ GeV and $\tan \beta = 100$; III(c) $M_{H^\pm} = 450$ GeV and $\tan \beta = 150$; III(d) $M_{H^\pm} = 600$ GeV and $\tan \beta = 200$.

$E_\nu(\text{eV})$	$\sigma_{H^+}^{tot}/\sigma_{sm}^{tot}$			
	I(a)	I(b)	I(c)	I(d)
10^{14}	0.079	0.111	0.131	0.141
10^{15}	0.111	0.198	0.286	0.353
10^{16}	0.123	0.256	0.429	0.596
10^{17}	0.125	0.284	0.519	0.775
10^{18}	0.123	0.298	0.576	0.899
10^{19}	0.119	0.306	0.617	0.995
10^{20}	0.109	0.308	0.659	1.100

TABLE IV: $\sigma_{H^+}^{tot}(\nu_\tau + \mathcal{N} \rightarrow \tau^- + X)/\sigma_{sm}^{tot}(\nu_\tau + \mathcal{N} \rightarrow \tau^- + X)$ as a function of E_ν , with $E_{\mathcal{N}} = M_{\mathcal{N}}$ for the cases: I(a) $M_{H^\pm} = 90$ GeV and $\tan \beta = 60$; I(b) $M_{H^\pm} = 150$ GeV and $\tan \beta = 100$; I(c) $M_{H^\pm} = 225$ GeV and $\tan \beta = 150$; I(d) $M_{H^\pm} = 300$ GeV and $\tan \beta = 200$.

$E_\nu(\text{eV})$	$\sigma_{H^+}^{tot}/\sigma_{sm}^{tot}$			
	II(a)	II(b)	II(c)	II(d)
10^{14}	0.027	0.040	0.045	0.047
10^{15}	0.040	0.082	0.112	0.132
10^{16}	0.046	0.118	0.189	0.254
10^{17}	0.047	0.139	0.245	0.358
10^{18}	0.047	0.151	0.284	0.436
10^{19}	0.046	0.160	0.315	0.499
10^{20}	0.043	0.168	0.348	0.571

TABLE V: $\sigma_{H^+}^{tot}(\nu_\tau + \mathcal{N} \rightarrow \tau^- + X)/\sigma_{sm}^{tot}(\nu_\tau + \mathcal{N} \rightarrow \tau^- + X)$ as a function of E_ν , with $E_{\mathcal{N}} = M_{\mathcal{N}}$ for the cases: II(a) $M_{H^\pm} = 100$ GeV and $\tan \beta = 50$; II(b) $M_{H^\pm} = 200$ GeV and $\tan \beta = 100$; II(c) $M_{H^\pm} = 300$ GeV and $\tan \beta = 150$; II(d) $M_{H^\pm} = 400$ GeV and $\tan \beta = 200$.

$E_\nu(\text{eV})$	$\sigma_{H^+}^{tot}/\sigma_{sm}^{tot}$			
	III(a)	III(b)	III(c)	III(d)
10^{14}	0.007	0.009	0.009	0.010
10^{15}	0.012	0.022	0.028	0.031
10^{16}	0.016	0.037	0.056	0.072
10^{17}	0.018	0.048	0.082	0.116
10^{18}	0.019	0.056	0.102	0.152
10^{19}	0.019	0.062	0.118	0.184
10^{20}	0.019	0.069	0.137	0.220

TABLE VI: $\sigma_{H^+}^{tot}(\nu_\tau + \mathcal{N} \rightarrow \tau^- + X)/\sigma_{sm}^{tot}(\nu_\tau + \mathcal{N} \rightarrow \tau^- + X)$ as a function of E_ν , with $E_{\mathcal{N}} = M_{\mathcal{N}}$ for the cases: III(a) $M_{H^\pm} = 150$ GeV and $\tan \beta = 50$; III(b) $M_{H^\pm} = 300$ GeV and $\tan \beta = 100$; III(c) $M_{H^\pm} = 450$ GeV and $\tan \beta = 150$; III(d) $M_{H^\pm} = 600$ GeV and $\tan \beta = 200$.

$E_\nu(\text{eV})$	$\sigma_{H^+}^{tot}(\text{cm}^2)$					
	all quarks	bottom	strange	anti-charm	down	anti-up
10^{14}	9.40×10^{-36}	9.37×10^{-36}	1.67×10^{-38}	1.20×10^{-38}	3.15×10^{-40}	8.97×10^{-41}
10^{15}	9.06×10^{-35}	9.03×10^{-35}	1.25×10^{-37}	9.97×10^{-38}	1.35×10^{-39}	6.12×10^{-40}
10^{16}	4.96×10^{-34}	4.95×10^{-34}	5.45×10^{-37}	4.86×10^{-37}	3.18×10^{-39}	2.40×10^{-39}
10^{17}	1.76×10^{-33}	1.76×10^{-33}	1.67×10^{-36}	1.57×10^{-36}	7.26×10^{-39}	6.86×10^{-39}
10^{18}	4.96×10^{-33}	4.95×10^{-33}	4.27×10^{-36}	4.10×10^{-36}	1.73×10^{-38}	1.72×10^{-38}
10^{19}	1.22×10^{-32}	1.22×10^{-32}	9.93×10^{-36}	9.60×10^{-36}	3.96×10^{-38}	3.95×10^{-38}
10^{20}	2.72×10^{-32}	2.71×10^{-32}	2.14×10^{-35}	2.07×10^{-35}	8.45×10^{-38}	8.45×10^{-38}

TABLE VII: Contribution to $\sigma_{H^+}^{tot}$ from the different allowed initial quarks as a function of E_ν , with $E_{\mathcal{N}} = M_{\mathcal{N}}$, taking $M_{H^\pm} = 400$ GeV and $\tan \beta = 200$.

$E_\nu(\text{eV})$	$\langle y \rangle_{sm}^{CC}$	$\langle y \rangle_{2hdm}^{CC}$			
		I(a)	I(b)	I(c)	I(d)
10^{14}	0.355	0.383	0.394	0.401	0.405
10^{15}	0.289	0.332	0.362	0.388	0.407
10^{16}	0.255	0.305	0.349	0.394	0.430
10^{17}	0.234	0.286	0.339	0.397	0.443
10^{18}	0.218	0.272	0.330	0.396	0.449
10^{19}	0.204	0.258	0.321	0.394	0.453
10^{20}	0.180	0.232	0.302	0.386	0.452

TABLE VIII: Mean inelasticity parameter for charged current interaction $\langle y \rangle^{CC}$ as a function of E_ν , with $E_{\mathcal{N}} = M_{\mathcal{N}}$. We compare $\langle y \rangle_{sm}^{CC}$ with $\langle y \rangle_{2hdm}^{CC}$ by taking: I(a) $M_{H^\pm} = 90$ GeV and $\tan \beta = 60$; I(b) $M_{H^\pm} = 150$ GeV and $\tan \beta = 100$; I(c) $M_{H^\pm} = 225$ GeV and $\tan \beta = 150$; I(d) $M_{H^\pm} = 300$ GeV and $\tan \beta = 200$.